Halide Dependence of the Halorhodopsin Photocycle as Measured by Time-Resolved Infrared Spectra

M. Shane Hutson,* Sergey V. Shilov,† Richard Krebs,† and Mark S. Braiman†

*Biophysics Program, University of Virginia Health Sciences Center 456, Charlottesville, Virginia 22908; and †Department of Chemistry, Syracuse University, Syracuse, New York 13244-4100 USA

ABSTRACT Time-resolved Fourier transform infrared (FTIR) difference spectra of the halorhodopsin (hR) photocycle have been collected from 3 μs to 100 ms in saturating concentrations of KCl or KBr. Kinetic analysis of these data revealed two decay processes, with time constants of $\tau_1 \simeq 150$ μs and $\tau_2 \simeq 16$ ms in the presence of either halide, with τ_2 describing the return to the starting (hR) state. Comparison to previous low-temperature FTIR spectra of hR intermediates confirms that characteristic hK and hL spectral features are both present before the τ_1 decay, in a state previously defined as hK_L (Dioumaev, A., and M. Braiman. 1997. *Photochem. Photobiol.* 66:755–763). However, the relative sizes of these features depend on which halide is present. In Br^-, the hL features are clearly more dominant than in Cl^-. Therefore, the state present before τ_1 is probably best described as an hK_L/hL_1 equilibrium, instead of a single hK_L state. Different halides affect the relative amounts of hK_L and hL_1 present, i.e., Cl^- produces a much more significant back-reaction from hL_1 to hK_L than does Br^-. The halide dependence of this back-reaction could therefore explain the halide selectivity of the halorhodopsin anion pump.

INTRODUCTION

Halorhodopsin (hR), a 274-residue protein found in the plasma membrane of *Halobacterium salinarium*, functions as a light-driven chloride pump (Schobert and Lanyi, 1982). A recently published high-resolution crystal structure of this protein (Kolbe et al., 2000) has revealed a single well-defined Cl^- binding site, opening the door to an atomic-level understanding of the mechanism of transmembrane anion transport in this system.

The dynamical properties of hR have been studied mostly through time-resolved spectroscopic measurements. Upon absorption of a photon, the covalently attached all-*trans* retinylidene chromophore isomerizes to 13-*cis* (Lanyi, 1984). After this isomerization, the chromoprotein decays to the initial state through a series of photocycle intermediates denoted hK, hL, hN, and hO by analogy with the intermediates of the bacteriorhodopsin (bR) photocycle (Váró et al., 1995b). The net result of the photocycle is the transport of a chloride ion from the external medium into the cytoplasm.

The sequence of intermediates in the hR photocycle and their interconversions have been the subject of numerous studies (Váró et al., 1995a, b; Hazemoto et al., 1984; Zimányi and Lanyi, 1989a, b; Zimányi et al., 1989; Spencer and Dewey, 1990; Ames et al., 1992; Dioumaev and Braiman, 1997a). The most complete description of the hR photocycle, from transient visible spectra (Váró et al., 1995b), considered the heterogeneity of the initial hR state: chloride-free, chloride-bound all-*trans* and chloride-bound 13-*cis*. As originally proposed (Váró et al., 1995b), the all-*trans* photocycle of the *H. salinarium* protein was described as

$$hR + h\nu \rightarrow hK \leftrightharpoons hL_1 \leftrightharpoons hL_2 \leftrightharpoons hN \rightarrow hR,$$

including significant back-reactions among the photointermediates (Váró et al., 1995b). Although the hL_1 and hL_2 states were spectroscopically identical, the presence of these two substates was necessary to fit the observed kinetics (Váró et al., 1995b). The rate at which hL_2 and hN reach equilibrium was fast compared to the $hL_1 \leftrightharpoons hL_2$ equilibrium, and thus the model with four intermediates resulted in only three experimentally determined time constants at room temperature and 2 M NaCl (Váró et al., 1995b). The time constants were 400 ns, 91 μs, and 10 ms describing, respectively, the equilibration of hK and hL_1, the equilibration of these states with hL_2 and hN, and the decay back to the original hR state (Váró et al., 1995b).

Similar experiments with hR from *Natronobacterium pharaonis* provided evidence that a red-shifted hO state was also present in the all-*trans* photocycle (Váró et al., 1995a). Thus, the model was modified to

$$hR + h\nu \rightarrow hK \leftrightharpoons hL_1 \leftrightharpoons hL_2 \leftrightharpoons hN \leftrightharpoons hO \rightarrow hR,$$

to accommodate the hO state. However, at molar chloride concentrations, no significant amount of hO accumulates (Váró et al., 1995a). Under these conditions, the original model based on the *H. salinarium* protein (Váró et al., 1995b) is sufficient to describe the photocycle.

The only previous attempt to model the hR photocycle from time-resolved FTIR data (Dioumaev and Braiman, 1997a) came to a slightly different conclusion. The obser-

Received for publication 15 May 2000 and in final form 20 December 2000.

Address reprint requests to Dr. Mark Braiman, Dept. of Chemistry, Rm. 1-014 Center for Science and Technology, Syracuse University, Syracuse, NY 13244-4100. Tel.: 315-443-4691; Fax: 315-443-4070; E-mail: mbraiman@syr.edu.

M. Shane Hutson's present address is Duke University FEL, Durham, NC 27708.

0006-3495/01/03/1452/14 $2.00

vation of strong hydrogen-out-of-plane (HOOP) vibrational modes from the retinylidene chromophore that decayed with time constants of 280 ns and 300 μs led to a unidirectional model of the early photocycle with two different hK states:

$$\mathrm{hR} + h\nu \rightarrow \mathrm{hK_E} \rightarrow \mathrm{hK_L} \rightarrow \mathrm{hL} \rightarrow \cdots \rightarrow \mathrm{hR}$$

The $\mathrm{hK_E}$ (early K) and $\mathrm{hK_L}$ (late K) states were named by analogy with the substates of the early bR photocycle (Dioumaev and Braiman, 1997b). Although a back-reaction from hL to $\mathrm{hK_L}$ was not explicitly included in the model, it was noted that such a reaction could contribute to the long-lived HOOP modes (Dioumaev and Braiman, 1997a).

Although the function of hR under physiological conditions is the active transport of chloride, the protein is also capable of transporting other halides. Br^- is transported with equal efficiency to Cl^-, and I^- to a somewhat lesser extent (Schobert et al., 1983; Steiner et al., 1984). Large polyatomic anions, such as sulfate and thiocyanate, can bind to the protein similarly to the halides, but they are not transported and do not produce the blue-shifted hL state upon photoexcitation (Steiner et al., 1984). The smaller nitrate anion shows an intermediate level of transport and supports hL formation in ~50% of the photocycling protein (Steiner et al., 1984).

The ability of hR to bind and transport different halides was used previously to address the nature of its halide binding site(s). Fourier transform infrared (FTIR) difference spectra of hL-hR were measured by phototrapping the hL state at −20°C in the presence of Cl^-, Br^-, and I^-. Examination of these spectra for indications of a direct interaction of the bound halide with protein residues revealed several bands with frequencies that shifted significantly as a function of the halide that was present (Walter and Braiman, 1994; Braiman et al., 1994). The halide dependence of three of these frequencies (1695, 1611, and 1169 cm^{-1}) was attributed to an interaction of arginine with the halide in the hR state (Braiman et al., 1994). Halide effects on two other frequencies (1642 and 1631 cm^{-1}) were attributed to halide interactions with the protonated Schiff base in both hR and hL states (Walter and Braiman, 1994).

To further examine halide-dependent effects in the hR photocycle, we have measured time-resolved FTIR data, from 3 μs to 100 ms, of hR in the presence of saturating concentrations of KCl or KBr. Although halide-dependence usually refers to a dependence upon the concentration of a halide, in this report the term will be reserved to describe effects that depend upon the identity of the halide present. Similar time-resolved FTIR experiments in KI were not possible due to lower long-term photochemical stability of the sample.

The measured time constants agree well with both the previous visible and FTIR studies. However, the halide dependence of spectral differences before the first observed decay suggests that a significant hL → hK back-reaction is responsible for the long-lived intense HOOP modes, and furthermore that the extent of this back-reaction is dependent on which halide is present. Variable effects of this back reaction on low-temperature FTIR spectra might cause some of the previously observed halide-dependent frequency shifts (Walter and Braiman, 1994; Braiman et al., 1994). In light of this, the halide-dependent vibrational band assignments in the hR → hL difference spectra, and the models for chloride binding sites in the protein built from these data, must be reexamined.

MATERIALS AND METHODS

Protein samples

The hR protein used in these experiments was harvested from the bR-deficient, hR-overproducing strain D2 of *H. salinarium*, a gift from Prof. D. Oesterhelt of the Max Planck Institute for Biochemistry, Martinsried, Germany (Heymann et al., 1993). The hR-enriched membranes were isolated as described previously (Bivin and Stoeckenius, 1986). The protein was then solubilized in 7% cholate, purified on a Phenylsepharose (Pharmacia, Piscataway, NJ) column and reconstituted into vesicles of purified halobacterial lipids as described previously (Walter and Braiman, 1994; Duschl et al., 1988). Reconstituted hR samples were then pelleted and resuspended at least five times with a 10-fold excess of 10 mM HEPES at pH 7 containing either 500 mM KCl or 500 mM KBr. After the final centrifugation the supernatant was aspirated until ~0.5 volumes of it remained (relative to the pellet). This remaining supernatant was then used to resuspend the hR vesicle pellet at a concentration of ~0.1 mM. FTIR samples were made from these suspensions with slight modifications to previously published procedures (Braiman et al., 1987; Dioumaev and Braiman, 1997b). Approximately 10 μl of the concentrated hR vesicle suspension was pipetted onto a BaF_2 window and spread over a ~1 cm^2 area of the window while partially drying under a gentle stream of dry air. The volume of the sample was reduced by 5–10 times upon drying, so that the final halide concentration in the sample was >2 M, and the final water content of the sample was ~50% by weight. After the partial air-drying, a second BaF_2 window coated around its edge with vacuum grease was lowered onto the sample to squeeze it to a uniform thickness and to seal it from further changes in water content.

Time-resolved FTIR measurements

Time-resolved FTIR data were collected on a Nicolet Magna-IR 860 Spectrometer in step-scan mode with a 20 MHz photovoltaic HgCdTe-A detector equipped with both AC- and DC-coupled outputs. A pulsed, frequency-doubled Nd^+-YAG laser (532 nm, 10 mJ cm^{-2}) was used to initiate the photocycle. Spectra were recorded with 8 cm^{-1} resolution over a Nyquist bandwidth of 0–1975 cm^{-1}. A long-pass optical filter (2000 cm^{-1} cutoff) was placed in the infrared beam between the sample and detector to block scattered light from the Nd^+-YAG laser and to prevent aliasing from infrared intensity above 1975 cm^{-1}.

Transient signals at each of 640 mirror positions were collected simultaneously in AC- and DC-coupled modes. The AC-coupled signal was recorded with a time resolution of 100 ns using an external, 12-bit, PAD1232 board (Spectrum GmbH, Siek, Germany) in a personal computer, under the control of a home-modified Matlab driver. The AC-coupling time constant of this detector output was ~800 μs. The Nicolet spectrometer's internal digitizer was used to record the DC-coupled signal from 0.1 to 10 ms at a time resolution of 100 μs or from 1–100 ms at a time resolution of 1 ms, as well as the static DC level during 100 ms immediately preceding each laser flash. The AC-coupled spectra were averaged on

a pseudo-logarithmic time scale and corrected for the exponential instrumental decay by comparison with the simultaneously measured DC-coupled spectra. The DC-coupled spectra were also averaged on a roughly logarithmic time scale. The three data sets (100 ns to 500 μs, 100 μs to 10 ms, and 1 ms to 100 ms) were spliced together. With only 100 flashes per mirror position, the earliest spectra were not of sufficient quality to include in the subsequent analysis. Thus the data recorded before 3 μs were discarded. The final data sets in both KCl and KBr consisted of 134 spectra covering the time range from 3 μs to 100 ms after the flash, with roughly logarithmic spacing (30 spectra per decade of time).

Alternatively, to improve the data quality in the time window from 10 μs to 1 ms, some spectra were measured in an AC-coupled mode with the spectrometer's internal digitizer. An 11-KHz high-pass filter on this board greatly increased the signal-to-noise ratio, but the presence of both high- and low-pass filters prevented fitting these data to sums of exponential decays.

Data analysis

Principal components analysis (PCA) was performed using the PLSplus/IQ suite of programs with GRAMS/32 software (Galactic Industries, Salem, NH). Each set of time-resolved FTIR spectra was truncated to the region 950–1800 cm^{-1} before PCA. The result of PCA was a reduced representation of the data $\Delta A(\bar{\nu}, t) = \sum_{i=1}^{Nf} F_i(\bar{\nu}) \sqrt{\lambda(i)} S_i(t)$, where $F_i(\bar{\nu})$ is the spectrum of each factor, $S_i(t)$ are the time-resolved scores for each factor, and $\lambda(i)$ is the eigenvalue, which is also the variance accounted for by factor i. This representation is mathematically equivalent to singular value decomposition (Chen and Braiman, 1991; Hessling et al., 1993). The number of factors to keep for subsequent analysis was determined from an F-test of the reduced eigenvalues at a significance threshold of 0.98, with the ith reduced eigenvalue $REV(i)$ defined as

$$REV(i) = \frac{\lambda(i)}{(n - i - 1)(p - i - 1)},$$

where i is the factor number, n is the total number of spectra in the data set (i.e., the total number of time points), and p is the number of data points in each spectrum. Using this criteria usually results in a model that is slightly overfit (Malinowski and Howery, 1980). The time-resolved score for each factor was then weighted by $\sqrt{\lambda(i)}$. The reduced data set, consisting of the variance-weighted time-resolved scores of the retained factors, was then subjected to a global multiexponential fit with the program FITEXP (Dioumaev, 1997; Sharonov et al., 1991). The number of exponentials chosen to model the data was based on an F-test of the residual variance with a significance threshold of 0.99. The resultant fit

$$\sqrt{\lambda(i)} S_i(t) = \sum_{j=1}^{Ne} C_{ij} e^{-t/\tau(j)}$$

was used to construct the amplitude spectra $B_j(\bar{\nu})$ from the factor spectra according to

$$B_j(\bar{\nu}) = \sum_{i=1}^{Nf} C_{ij} F_i(\bar{\nu}).$$

The use of amplitude spectra to describe time-resolved spectral data has been discussed in detail previously (Chizhov et al., 1996).

RESULTS

Fig. 1 shows individual time slices from a series of time-resolved FTIR spectra collected on hR. The retinal C═C and C—C stretch difference bands at 1523(−), 1209(−), 1189(+), and 1168(−) cm^{-1} are indicative of photoproducts of the all-*trans* photocycle (Rothschild et al., 1988). The lack of a negative band at 1185 cm^{-1} and the presence of only one depletion band for the retinal C═C stretch (1523 cm^{-1}) indicate that there is little contribution to these spectra from 13-*cis* photocycle intermediates (Fodor et al., 1987; Ames et al., 1992).

It is apparent that a spectral transition is taking place between 60 and 180 μs. The principal features of this transition are a loss of intensity of the positive HOOP mode at 965 cm^{-1} (Dioumaev and Braiman, 1997a; Gerscher et al., 1997; Pande et al., 1989), an intensity increase for the positive band at 1556 cm^{-1}, with contributions from amide II and retinal C═C stretch modes (Chon et al., 1999), and an intensity increase of the Schiff base C═NH^+ stretch mode at 1642 cm^{-1} (Walter and Braiman, 1994; Gerscher et al., 1997; Pande et al., 1989). Taken together, these changes imply a loss of hK features and a gain of hL features during the transition.

In general, these observations are consistent with earlier time-resolved FTIR spectra of hR on this time scale (Dioumaev and Braiman, 1997a). However, the intensity of the 965 cm^{-1} HOOP mode is less than in the earlier spectra and the intensity of the band at 1556 cm^{-1} is greater. These differences could be related to the use of different sample purification methods. Sucrose density gradient fractionation of native membrane fragments was used in the earlier work (Dioumaev and Braiman, 1997a), whereas column purification in detergent solution, followed by reconstitution with lipids, was used here.

Due to the coverage of a limited time domain, only to 1 ms, and the presence of complicating high- and low-pass filters, the spectra in Fig. 1 were not amenable to further analysis via multiexponential fitting to describe the observed transition.

Kinetic analysis

To examine the transitions of the later stages of the hR photocycle, spectra were collected from 3 μs to 100 ms of suspensions containing saturating concentrations of either KCl or KBr. PCA revealed five significant factors in the presence of either KCl or KBr. However, it is clear that the last two to three factors had significant contributions from 60 Hz noise up to the fourth harmonic. The presence of this sort of artifact in time-resolved FTIR data has been previously documented (Rödig and Siebert, 1999). However, when the time courses from the PCA were variance-weighted the contributions from these 60-Hz artifacts were small enough to permit multiexponential fitting of the data. The resulting factor spectra and time courses from this analysis are presented in Fig. 2, *A* and *B* for KCl, and Fig. 2, *C* and *D* for KBr.

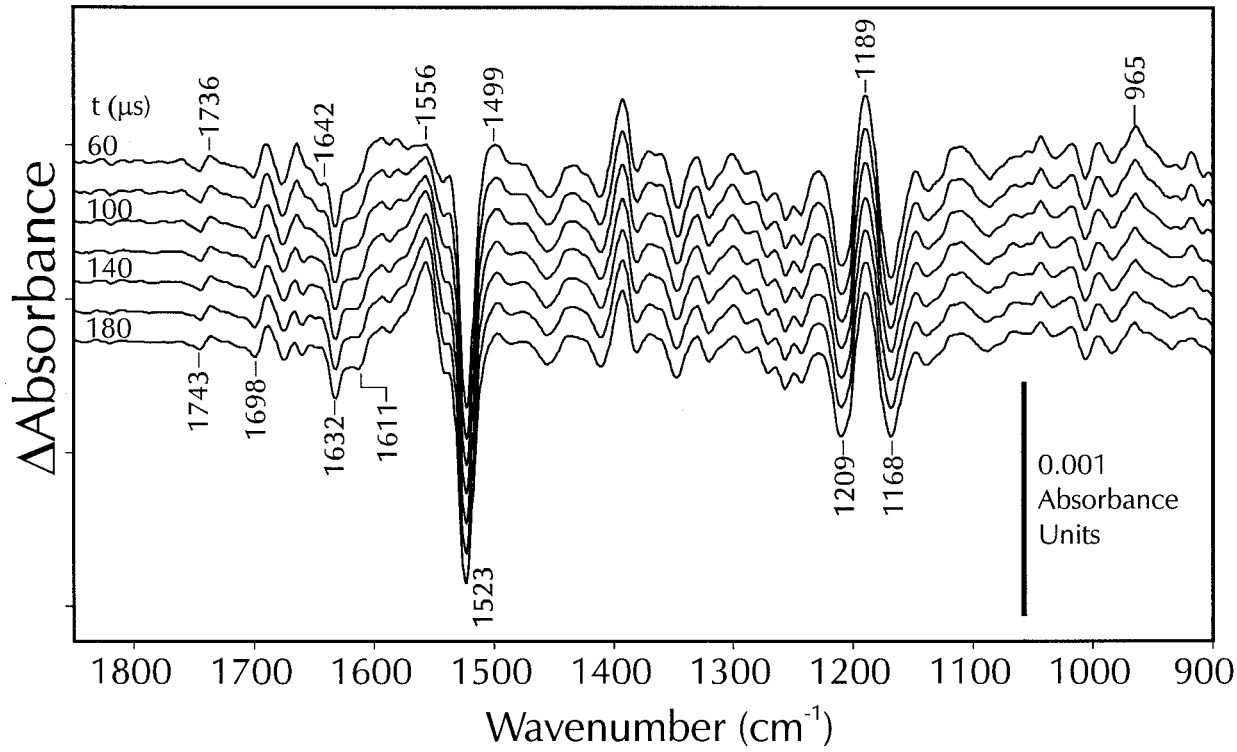

FIGURE 1 Individual time-resolved spectra of a transition between hR photoproducts at 25°C in a saturated KCl solution (pH = 7) with the spectrometer internal digitizer at a time resolution of 10 μs. The topmost spectrum shown here corresponds to 60 μs after the flash. The remaining spectra are spaced in 20-μs increments.

In the presence of KCl, multiexponential fitting described the data with only two time constants, $\tau_1 = 146 \pm 65$ μs and $\tau_2 = 15.3 \pm 3.5$ ms. The *F*-test significance of a third exponential was only 95.3%. To add a fourth dropped the significance down to 5.5%. However, the third time constant was only 0.2 μs, faster than the data (measured with 100 ns temporal resolution) could actually support, but very similar to that reported earlier, 0.3 μs (Dioumaev and Braiman, 1997a). In addition, extending the fit to three exponentials produced no significant change in the amplitude spectra or time constants of the longer decays. The amplitude spectra for the two fitted decays in KCl are shown in Fig. 3.

Analysis of the spectra collected in a saturated KBr solution resulted in a similar fit. The *F*-test significances for adding the second, third, fourth, and fifth factors were 99.1%, 99.8%, 97.1%, and 6.6%, respectively. It would seem that up to four exponentials were significant. However, once again, the two longest time constants and the associated amplitude spectra did not change significantly as more exponentials were added to the fit. Likewise, the additional time constants were too small (0.2 and 0.4 μs) to be described accurately by the measured data. Thus, for hR in KBr solution, the two-exponential fit resulted in time constants of $\tau_1 = 152 \pm 96$ μs and $\tau_2 = 16.7 \pm 4.8$ ms. The corresponding amplitude spectra are shown in Fig. 3. Within experimental error, the fitted time constants are equivalent to those seen in KCl. Thus, the decay processes in both Cl^- and Br^- will be referred to as the τ_1, or 150-μs, and τ_2, or 16-ms, decays.

The amplitude spectrum for the τ_1 decay in KCl faithfully represents changes observable in unfitted spectra between 60 and 180 μs (e.g., Fig. 1). The loss of intensity of the HOOP mode in Fig. 1 corresponds to the presence of a positive band at 974 cm^{-1} in the 150-μs amplitude spectrum, Fig. 3 *A*. The intensity increase of the amide II mode at 1556 cm^{-1} is also clearly identifiable as a negative band in Fig. 3 *A*. Thus, the largest features in the 150-μs amplitude spectrum correspond to a loss of spectral features previously attributed to hK (Rothschild et al., 1988; Dioumaev and Braiman, 1997a), and a gain of features previously attributed to hL (Rothschild et al., 1988; Walter and Braiman, 1994; Chon et al., 1999; Braiman et al., 1994). Additional evidence for this generalization is seen in the retinal C—C stretch modes at 1192 and 1166 cm^{-1} in the τ_1 spectrum, which correspond to a decrease in absolute intensity for the respective difference bands upon conversion of hK to hL (Rothschild et al., 1988). Furthermore, a band at 1695 cm^{-1}, previously attributed to an Arg-108 C═N stretch in hL (Braiman et al., 1994), is normally absent from low-temperature FTIR spectra of hK, while the band at 1624 cm^{-1} is much larger in hK spectra than in hL (Rothschild et

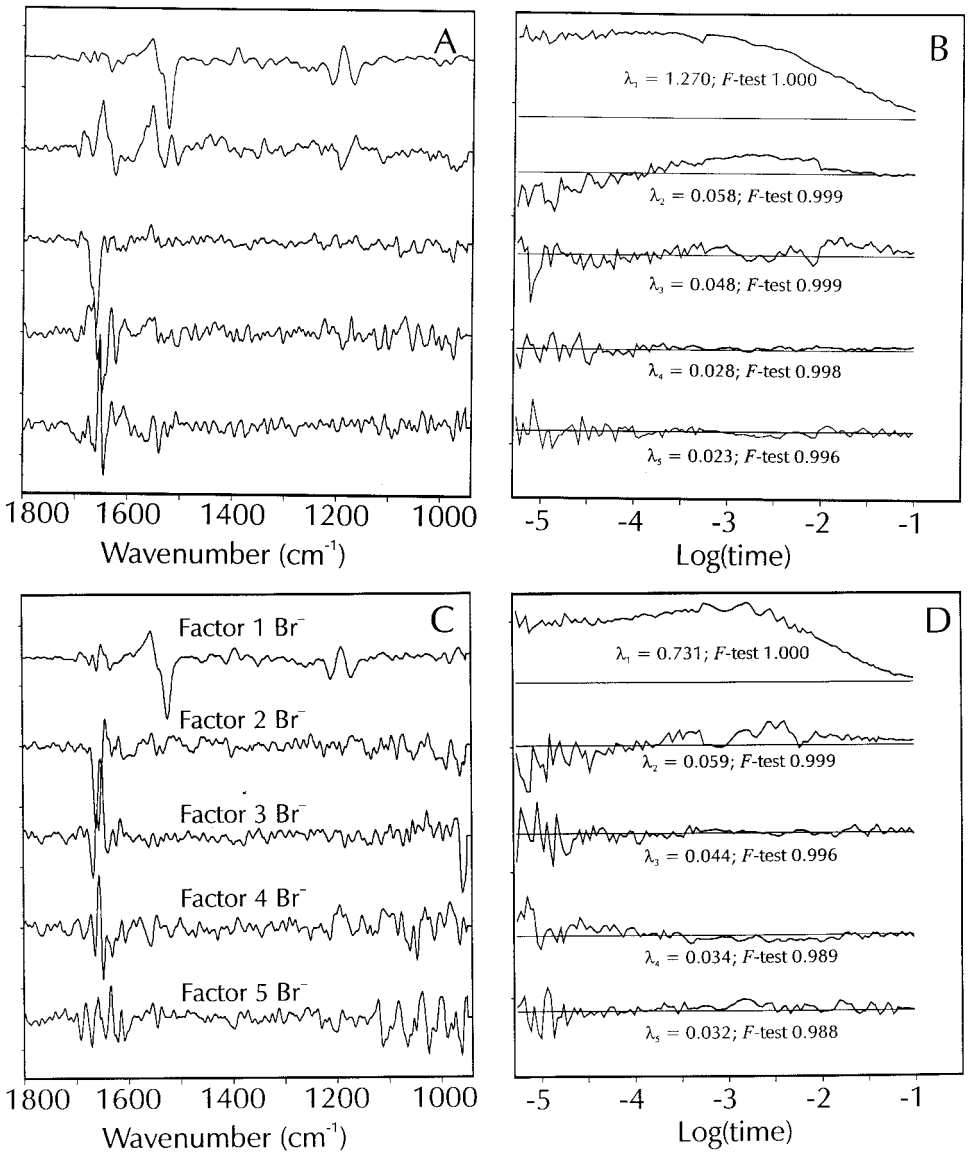

FIGURE 2 PCA results for time-resolved FTIR spectra of hR in the presence of saturating concentrations of KCl (*A* and *B*) or KBr (*C* and *D*). The variance weighting provided by $\sqrt{\lambda_i}$ has been transferred from the factor spectra (*A* and *C*) to the time courses (*B* and *D*). Eigenvalues and *F*-test significances for each factor are listed with the time courses. The next factor in KCl had $\lambda_6 = 0.013$ and an *F*-test score of 0.976. In KBr, the values were $\lambda_6 = 0.025$ and 0.974.

al., 1988). Thus, in the 150-μs amplitude spectrum (Fig. 3 *A*), there is clear evidence that the τ_1 process in KCl describes an hK→hL decay.

In contrast, the τ_1 amplitude spectrum in KBr is missing many of these attributes. Positive hK features at 974, 1192, 1506, and 1624 cm^{-1} are absent or greatly reduced in intensity. The strongest hL features in the Br^- 150-μs amplitude spectrum (Fig. 3 *B*) remain, but at a reduced amplitude when compared to the data in Cl^- (Fig. 3 *A*). The pair of bands at 1695/1688 cm^{-1} and the negative band at 1556 cm^{-1} are approximately half as intense in Br^- as in Cl^-. Thus, the nature of the 150-μs decay in Br^- is much less clear than in Cl^-. Certainly, the involvement of an hK state in this transition is greatly reduced as compared to the 150-μs decay in Cl^-.

Although there are large halide-dependent differences in the τ_1 amplitude spectrum, the $\tau_2 = 16$ ms amplitude spectrum is very similar in Cl^- and Br^-. The τ_2 amplitude spectrum is nearly identical to difference spectra of hL measured at −20°C (Rothschild et al., 1988; Walter and Braiman, 1994; Chon et al., 1999; Braiman et al., 1994). Thus, this process represents the decay of the late photocycle intermediates, principally hL, back to the initial hR state.

To further investigate the discrepancy between the time-resolved FTIR data in Cl^- and Br^-, the spectra of states present before and after the τ_1 decay were computed for each halide. These spectra do not necessarily represent pure intermediates, but rather a mixture of intermediates present in each time regime. The state present after the τ_1 decay (Fig. 4 *B*) is given by the τ_2 amplitude spectra in Fig. 3, while the spectrum of the state present before the τ_1 decay (Fig. 4 *A*) is given by the sum of the τ_1 and τ_2 amplitude spectra in Fig. 3. Comparing Fig. 4, *A* and *B*, it is clear that

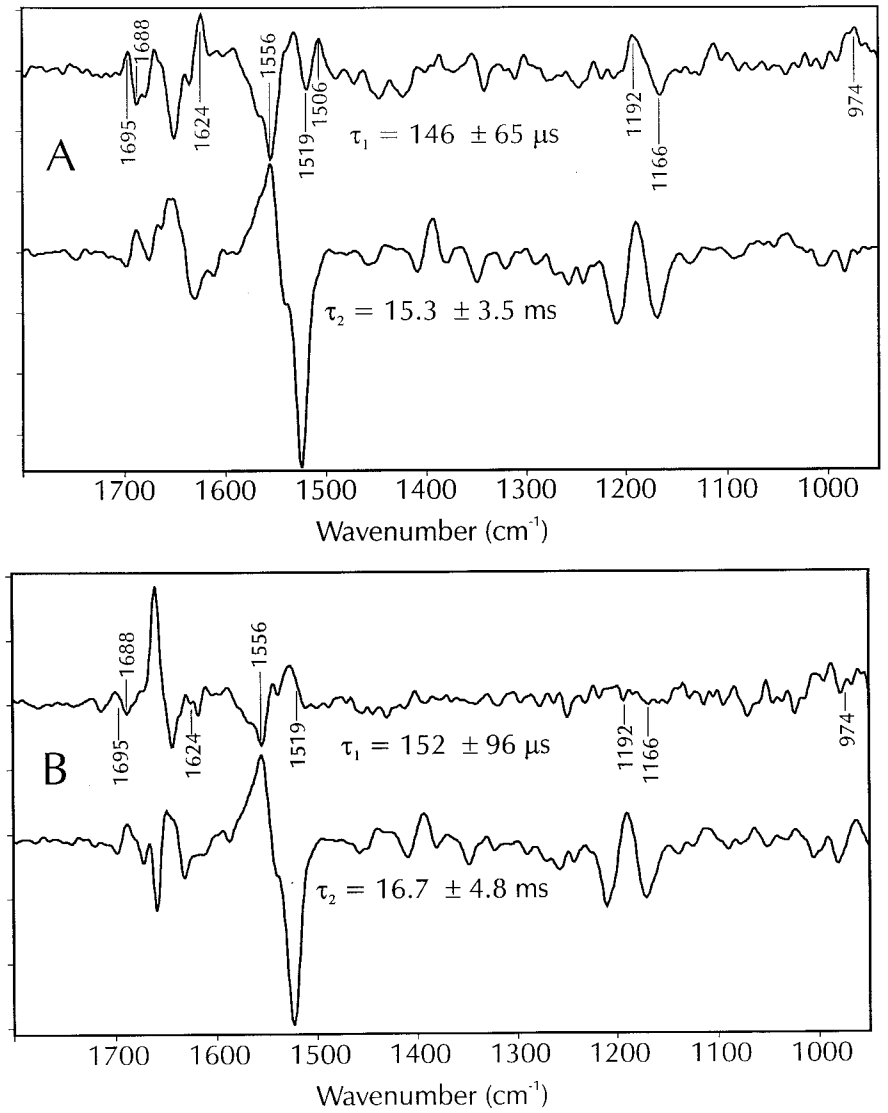

FIGURE 3 Amplitude spectra for the global multiexponential fit of the hR photocycle in the presence of saturating concentrations of KCl (*A*) or KBr (*B*). The associated time constant is listed with each amplitude spectrum.

difference spectra of the early photocycle intermediates are more halide-dependent than those of the later intermediates.

DISCUSSION

The present measurements of time-resolved FTIR spectra of the hR photocycle can be phenomenologically described by just two decay processes. As a starting point for applying photocycle models to the data, the photoproduct mixture present before τ_1 is designated as state 1 and that after τ_1 as state 2. It can be seen clearly from the superposition in Fig. 4 *B* that the spectra of state 2 are nearly identical in Cl^- and Br^-. Thus, the mixture of photointermediates that is present on the millisecond time scale and that decays back to the initial hR state is the same regardless of which halide is being transported.

The room-temperature difference spectra in Fig. 4 closely resemble those of hR intermediates phototrapped at −20°C, originally described as hR→hL difference spectra (Rothschild et al., 1988; Walter and Braiman, 1994; Chon et al., 1999; Braiman et al., 1994). Other workers have more recently designated this −20°C state as hL_B, in contrast to another hL state that can be trapped at −100°C (Chon et al., 1999). Based on room-temperature kinetic analyses of visible spectra of the hR photocycle, one would also expect a contribution of hN to the state present after τ_1. However, no FTIR spectrum of hN has been reported. Any possible contribution of hN to the observed spectra of this later photointermediate state (Fig. 4 *B*) cannot be evaluated.

Evaluation of kinetic models for the early hR photocycle

The multiexponential kinetic fits provide evidence of two significant time constants in the time range 3 μs–100 ms. This result supports the presence of only two photoproducts

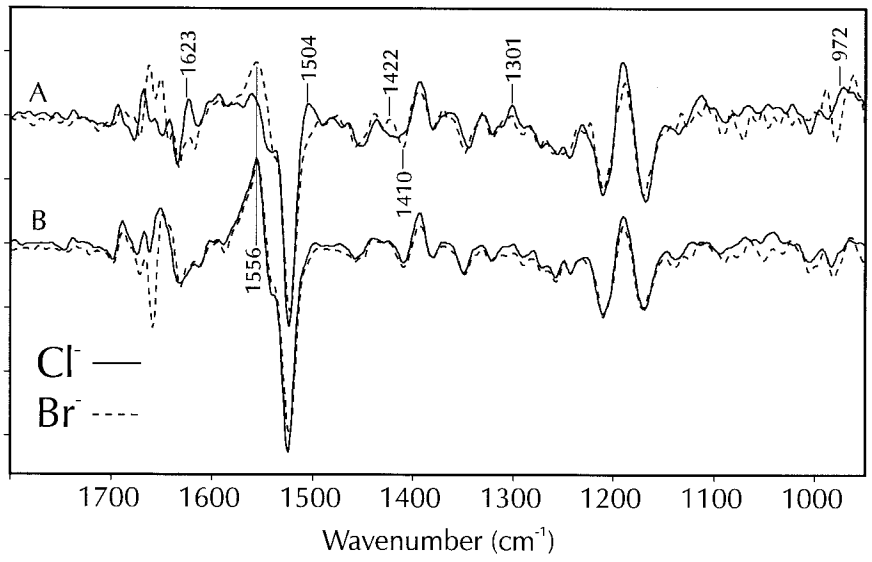

FIGURE 4 Calculated difference spectra of hR intermediates present before (*A*) and after (*B*) the τ_1 decay process in Cl^- (*solid line*) or Br^- (*dashed line*) solutions.

in this time range. The spectral features present indicate that, at least in the presence of Cl^-, these must be hK_L and hL. However, the PCA analyses shown in Fig. 2, performed separately on data sets measured in Cl^- or Br^-, do not unambiguously support that only two intermediates are present. Only the first two kinetic traces in each of Fig. 2, *B* and *D*, show plainly visible evidence of multiexponential decay behavior above the noise. However, the third kinetic trace in Fig. 2 *B* shows indications of an additional significant component. The factor spectra (Fig. 2, *A* and *C*) likewise show evidence of significant signals above the noise in the third–fifth components, and the presence of more than two intermediates is possibly supported by the *F*-test statistics.

However, PCA statistics can be adversely affected by performing the analysis simultaneously on spectral regions that have very different signal/noise ratios. Therefore, we repeated the PCA on the combined data sets (both in Cl^- and in Br^-), first removing the noisiest spectral regions (below 1100 cm^{-1} and between 1620 and 1680 cm^{-1}). The resulting factor spectra, shown in Fig. 5, provide clear evidence that three photointermediates are required to account for the two sets of spectra measured in this time range. In particular, the third factor spectrum has distinct features in the regions near 1200 cm^{-1} and 1500–1600 cm^{-1} that rise above the otherwise fairly uniform noise, whereas the fourth and fifth factors show only uniformly distributed noise. The presence of three significant components in the combined PCA analysis indicates the presence of a third photointermediate, i.e., one besides hK_L and hL, in these photocycles.

These results are unlikely to represent the presence of photoproduct(s) from a starting state with a 13-*cis* chromophore (Váró et al., 1995b). If such a parallel photocycle were present in significant amounts in our samples, we would expect to see clear evidence of more than one time constant in the range beyond 1 ms. In this time range, however, only the 15-ms time constant is detected, whether in the presence of Br^- or Cl^-. The chance is very low that the completion time of a photocycle originating from a 13-*cis* starting state would be indistinguishable from that of the all-*trans* hR photocycle, as is the chance that this 13-*cis* photocycle completion time would be too close to the 150-μs time constant to detect it.

The spectra of state 1 (Fig. 4 *A*) are much more dependent upon which halide is present than spectra of state 2. The spectrum of state 1 in Cl^- has bands present at 1301, 1504, and 1623 cm^{-1} that are much smaller in Br^-. The amide II band at 1556 cm^{-1} is much larger in the spectrum of state 1 in Br^- than in Cl^-. There is also a positive/negative band pair at 1422/1410 cm^{-1} in Br^- that is absent in Cl^-. In addition, in place of the positive HOOP mode band at 972 cm^{-1} in Cl^- there is a negative band at 979 cm^{-1} in Br^-.

The differences between the spectra of state 1 in Cl^- and Br^- (Fig. 4 *A*) are too great to attribute to a halide effect on band positions in a single intermediate. Rather, the data are better explained if a different mixture of intermediates is present in state 1 for each halide. The nature of the spectral differences implies that state 1 is a mixture of hK_L and hL states, with the equilibrium between hK_L and hL in state 1 favoring hK_L more strongly in Cl^- than in Br^-.

This description of state 1 parallels hR photocycle models that ascribed the long-lived hK-like intermediate to a significant $hL \rightarrow hK$ back-reaction (Váró et al., 1995a, b). However, a previous discussion of time-resolved FTIR data (Dioumaev and Braiman, 1997a) argued that a similar transition with $\tau \simeq 300$ μs represented a decay between hK_L and hL in reaction scheme I below:

$$hR + h\nu \rightarrow hK_E \rightarrow hK_L \rightarrow hL \rightarrow \cdots \rightarrow hR. \quad (I)$$

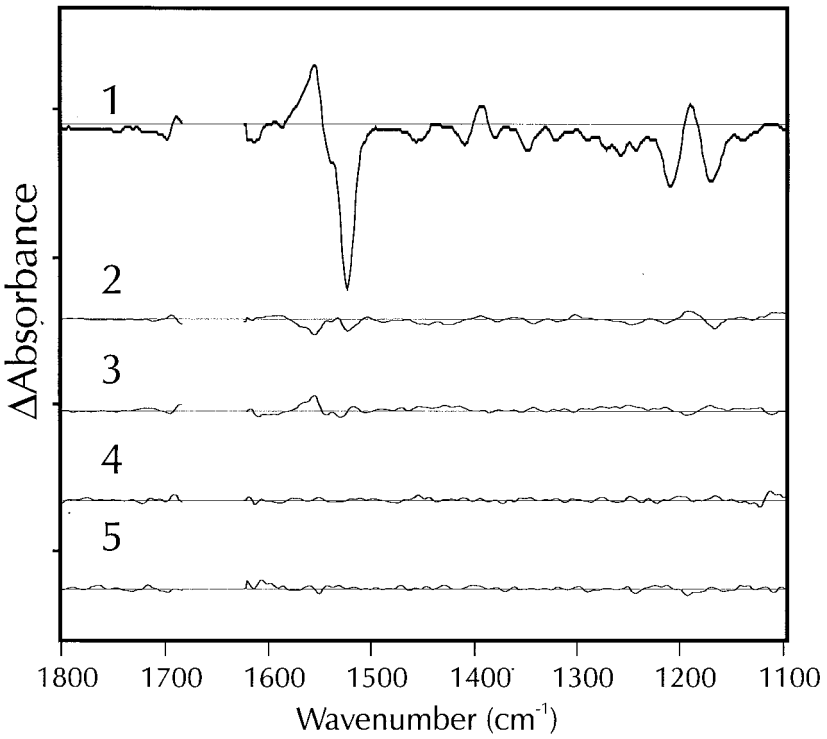

FIGURE 5 PCA results for combined Cl^- and Br^- spectral data sets covering the same time range (3 μs–100 ms) as in Fig. 2. In order to improve the statistics of the analysis and determine with more certainty the number of spectral components present, absorbance data matrices for both the Cl^- and Br^- over the range 1800–1100 cm^{-1} were appended to each other, excluding the region from 1620 to 1680 cm^{-1}. Then PCA was performed, yielding appended time courses (equivalent to the *V*-matrix of an SVD; not shown) and weighted factor spectra (equivalent to the *SU*-matrix of an SVD), the first five of which are shown here. Note that the relative vertical scaling of the factor spectra in this representation differs from Fig. 2 in that the variance weighting ($\sqrt{\lambda_i}$) has been transferred from the time courses (not shown) to the factor spectra. These $\sqrt{\lambda_i}$ values are 65.1, 11.3, 8.8, 7.4, 7.3; and the corresponding *F*-test scores are 1.0000, 0.9995, 0.9958, 0.9848, 0.9847.

This previous conclusion was driven by two lines of evidence. 1) Two time constants (280 ns and 300 μs) were necessary to describe the decay of the strong HOOP vibrational mode near 970 cm^{-1}, which is indicative of hK species. 2) The FTIR spectrum of the species present after the 280-ns decay was similar, but not identical, to what was certainly an hK species observed before this decay (Dioumaev and Braiman, 1997a). Although the signal/noise ratio of our submicrosecond data in the current measurements was not sufficient to measure the 280-ns decay process, our data confirm the other observations from this previous work. When measured in the presence of Cl^-, significant intensity is observed in a long-lived HOOP mode that decays on the 100-μs time scale. In addition, the species present before this decay has a spectrum with many other features indicative of an hK-like state.

However, upon substitution of Br^- for Cl^-, large spectral differences are observed in the species present before the τ_1 decay. It does not seem reasonable to conclude that the extent of these changes could be caused by halide-dependent effects on the bands of a single photointermediate. A more straightforward explanation of these differences is that a halide-dependent equilibrium of two photointermediates is present on this time scale. The FTIR spectrum of this mixture suggests that it is composed of both hK- and hL-like species. In support of this conclusion is the previous observation that the relative contribution of the nanosecond and microsecond processes to the HOOP mode decay was temperature-dependent (Dioumaev and Braiman, 1997a). It was speculated that this represented a possible $hK_L \rightarrow hK_E$ back-reaction. In light of the present data this is instead interpreted as a manifestation of an hK_L/hL equilibrium on the microsecond time scale. That is, the 300 μs phenomenological time constant most closely corresponds to a microscopic rate constant involving hL decay to its successor state, rather than decay of hK_L to hL. The latter microscopic rate constant contributes to, and can be reasonably approximated by, the phenomenological rate constant of ~280 ns.

The currently prevalent nomenclature of the immediate precusor to hL designates it simply as hK (Váró et al., 1995b). However, this usage would suggest that the highly twisted initial hK state, which is formed on the picosecond time scale (Polland et al., 1985), does not relax structurally before the 280-ns time scale, i.e., before a rapid hK $\rightleftharpoons$ hL equilibration corresponding to the reversible movement of a bound halide between two internal binding sites (see below). On the contrary, previous transient visible spectroscopy on the picosecond (Polland et al., 1985) and nanosecond (Zimányi et al., 1989) time scales indicates that the initial hK photoproduct state relaxes to a second state within 60 ns. It is therefore necessary to settle on a nomenclature that distinguishes between these hK states. Based on FTIR spectroscopy shown here and previously (Dioumaev and Braiman, 1997a), the structure of the latest hK state, which immediately precedes hL, is analogous to the immediate precursor to L in the bR photocycle, which we have previously designated as K_L (Dioumaev and Braiman, 1997a). Others have termed this bR photointermediate KL, based on the fact that some of its spectroscopic features are more "L-like" than "K-like," although this leads to a logical

conflict because this state (the immediate precursor to L detectable with time-resolved visible spectroscopy) was the one for which the term "K" was originally coined (Lozier et al., 1975). We will therefore continue to use the previously suggested nomenclature of hK_L (Dioumaev and Braiman, 1997a) to indicate the "late" or "last" hK intermediate, which relaxes directly to hL in the room-temperature photocycle and which is the structural analog of K_L (or KL) in the bR photocycle. It should be recognized nevertheless that the previously proposed formation and decay times of this hK_L intermediate (Dioumaev and Braiman, 1997a) are now concluded to have been incorrect.

The later photocycle intermediates

The observed time constants and the characteristics of the amplitude spectra lead to a phenomenological description of the sequence of hR intermediates as $hK_L/hL \rightarrow hL \rightarrow hR$. With the photoproduct mixture present on a 10-μs time scale attributed to a mixture of hK_L- and hL-like states, a third intermediate is necessary to construct a valid photocycle model. With this third photointermediate, the hR photocycle after ~1 μs and in the presence of high Cl^- concentrations could be equally well described as

$$hR + h\nu \rightarrow hK_L \leftrightharpoons hL \leftrightharpoons hX \rightarrow hR \qquad \text{(II)}$$

or

$$hR + h\nu \rightarrow hK_L \leftrightharpoons hL_1 \rightarrow hL_2 \rightarrow hR. \qquad \text{(III)}$$

Both of these schemes involve a submicrosecond equilibration of hK_L and hL states with rate constants that the present data cannot accurately determine. Because the photoproduct difference spectra in the millisecond time regime so closely resemble −20°C spectra of a blue-shifted hL state (Rothschild et al., 1988; Walter and Braiman, 1994; Chon et al., 1999; Braiman et al., 1994), the difference spectrum of the hX state (which may be either an hN or hO intermediate) in scheme II would necessarily be very similar to that of hL. In addition, transient visible spectroscopy has shown that a blue-shifted hL state is present on the millisecond time scale (Váró et al., 1995b; Zimányi and Lanyi, 1989b; Zimányi et al., 1989). Thus, the penultimate step in photocycle scheme II must be reversible. This requirement does not apply to scheme III, although the $hL_1 \rightleftharpoons hL_2$ step may be reversible without losing its ability to describe the observed kinetics.

A previous kinetic model from transient visible absorption changes of *H. salinarium* hR (Váró et al., 1995b) described the photocycle as

$$hR + h\nu \rightarrow hK \leftrightharpoons hL_1 \leftrightharpoons hL_2 \leftrightharpoons hN \rightarrow hR. \qquad \text{(IV)}$$

Only three time constants could be fitted using this model as the $hL_2 \rightleftharpoons hN$ step was kinetically unresolved. With a similar allowance for the submicrosecond equilibration of hK (i.e., hK_L) and hL_1, this model is also capable of describing the kinetics observed in our time-resolved FTIR spectra. The time constant fitted for the $hK \rightleftharpoons hL_1$ step in this previous study was 400 ns (Váró et al., 1995b). The τ_1 = 150 μs time constant seen in our data would correspond to the decay of an hK_L/hL_1 mixture to an hL_2/hN mixture. Our value for τ_1 agrees with the value of 91 μs from visible absorption data (Váró et al., 1995b).

Our τ_2 = 16 ms time constant would then correspond to the decay of an $hK_L/hL_1/hL_2$/hN mixture back to hR. The corresponding time constant from the previous transient visible absorption changes was 10 ms (Váró et al., 1995b). In accord with scheme IV, the spectrum of our state 1 (Fig. 4 *A*) would represent a mixture of hK_L and hL_1, and that of state 2 would represent a mixture of hL_2 and hN, with smaller contributions from hL_1 and hK_L. The presence of two hL substates on the millisecond time scale in this model somewhat relaxes the requirement that the FTIR difference spectra of hN and hL be very similar. Thus scheme IV, with two hL substates and an hN intermediate, is capable of accounting for the observed kinetic FTIR spectra of hR, although the full complexity of this model is not required.

In the formulation of scheme IV from transient visible spectra, Váró et al. (1995b) began with an ambiguity similar to that observed in our data, i.e., three observed time constants requiring three intermediates of unknown nature. However, the visible spectra of hR photointermediates can be subjected to constraints (specifically, limits on the half-width and relative intensities of chromophore absorption bands, as well as the requirement for a single peak for each hR intermediate in the visible spectral region) that allow one to decipher the ambiguities (Váró et al., 1995a, b; Zimányi and Lanyi, 1989b; Zimányi et al., 1989). The complexity of IR absorption difference spectra of hR, which arises from the presence of large numbers of overlapping spectral transitions, defeats the application of such constraints. That is, the IR data alone require only three photointermediates, not four, in the time range analyzed (3 μs–100 ms), and do not provide any independent support for the conclusion from visible spectroscopy of rapidly equilibrating hL and hN intermediates (Váró et al., 1995b).

Nevertheless, because scheme IV is the simplest photocycle model capable of fully describing the observed kinetic behavior of FTIR difference spectra and of satisfying the previously adopted framework of constraints on visible spectra (Váró et al., 1995b), it has been adopted as a framework for discussion in the remainder of this report. Thus, the spectrum of state 1 (Fig. 4 *A*) is attributed to a mixture of the longest-lived form of hK (i.e., hK_L) and hL_1, and the spectrum of state 2 (Fig. 4 *B*) is attributed mainly to an hL_2/hN mixture.

The model of Váró et al. (1995b) predicts that in the presence of Cl^-, the photoproduct mixture present after the 150-μs process (corresponding to our Fig. 4 *B*) should include some 17% of hK, whereas before this process (corresponding to our Fig. 4 *A*) it should be 50% hK. That is, the

amount of hK_L present in the solid-line spectrum of Fig. 4 *B* should be ~34% of that present in Fig. 4 *A*. The decrease in the sizes of signals at 1504 and 972 cm^{-1} is generally consistent with such a predicted decrease, considering our signal/noise ratio, the slightly different sample conditions that we used (which correspondingly gave slightly different kinetic constants), and the uncertainty of the shape of the hL spectrum underlying these particular bands. In summary, we see nothing in our current FTIR data that would contradict the details of the kinetic model of Váró et al. (1995b).

Comparison to low-temperature FTIR spectra of hL_A and hL_B

Recently, FTIR spectra of two different hL states have been measured by phototrapping hR intermediates at either −20 or −100°C (Chon et al., 1999). The major difference between these two states was a large, positive band at 1557 cm^{-1} indicative of a protein conformational change (Chon et al., 1999). These two cryogenic hL states were tentatively assigned to the hL_1 and hL_2 states of the room-temperature all-*trans* photocycle (Váró et al., 1995b; Chon et al., 1999). The time-resolved FTIR spectrum of the species we attribute to hL_2/hN (Fig. 4 *B*) corresponds very well with previous spectra of the hL_B state measured at −20°C (Rothschild et al., 1988; Walter and Braiman, 1994; Chon et al., 1999; Braiman et al., 1994).

However, it is harder to reconcile the low-temperature static FTIR difference spectrum of hL_A with the time-resolved spectra. In the presence of Cl^-, several of the smaller differences between the low-temperature hL_A and hL_B states are reproduced in the differences between the time-resolved hK/hL_1 (Fig. 4 *A*) and hL_2/hN spectra (Fig. 4 *B*). In particular, the relatively larger positive band at 1623 cm^{-1} and smaller negative band at 1697 cm^{-1} in the earlier time-resolved spectrum (Fig. 4 *A*) are also clearly evident as differences between hL_A at −100°C and hL_B at −20°C (Chon et al., 1999). In addition, the amide II band at 1557 cm^{-1} increases dramatically during the $\tau_1 = 150\ \mu s$ process in Cl^-, in analogy with a large difference between hL_A and hL_B (Chon et al., 1999). In contrast, in the presence of Br^- the spectrum displays much smaller changes at all of these band frequencies during the 150-μs decay. In Br^- the difference spectrum before this decay (Fig. 4 *A*) already has significant intensity in the 1557 cm^{-1} band, which then goes on to change very little during the decay (Fig. 4 *B*).

To identify the cryogenic states hL_A and hL_B with the room-temperature kinetic photointermediates hL_1 and hL_2, additional halide dependencies of the photocycle would have to be postulated. In particular, hL_2 would have to be present in significant amounts before the 150-μs decay in Br^-, but not in Cl^-. Thus, the state present before the τ_1 decay would be a halide-dependent mixture of hK_L, hL_1, and hL_2. Such an equilibrium could be accounted for by the adopted photocycle model with a reinterpretation of the observed time constants. If the extremely rapid equilibrium were moved from the $hL_2 \rightleftharpoons$ hN step to the $hL_1 \rightleftharpoons hL_2$ step, then the photocycle at high Cl^- concentrations would still be expected to exhibit only three phenomenological time constants on times scales longer than 100 ns (one of which would be too fast to define accurately from our measurements). In this case, the τ_1 process would represent the decay of an $hK_L/hL_1/hL_2$ mixture to a further equilibrium with hN. However, postulating that hL_2 equilibrates with hK_L and hL_1 before the 150-μs decay defeats the original purpose of introducing 2 hL substates into the photocycle model, which was to account for the change in the observed ratio of hK_L/hL from ~1:1 before this decay to ~1:2 afterward (Váró et al., 1995b). Thus, the low-temperature states, hL_A and hL_B (Chon et al., 1999), cannot reasonably be identified with the two hL substates proposed from kinetic analysis of transient visible spectra (Váró et al., 1995b).

Implications for halide interactions with hR

Time-resolved FTIR spectroscopy of the hR photocycle has provided evidence that changing the transported ion from Cl^- to Br^- strongly affects the hK_L/hL equilibrium ratio on the microsecond time scale. This finding is significant, as it implies that the halide-protein interaction is substantially altered in the transition from hK_L to hL. To understand this statement, it is helpful to define $\Delta\Delta G$ as

$$\Delta\Delta G = \Delta G(Cl^-, hK_L \rightarrow hL) - \Delta G(Br^-, hK_L \rightarrow hL).$$

During the transport of Br^-, the equilibrium attained before the 150-μs decay favors the hL state more strongly than during the transport of Cl^-, i.e.,

$$\Delta G(Br^-, hK_L \rightarrow hL) < \Delta G(Cl^-, hK_L \rightarrow hL)$$

and thus $\Delta\Delta G > 0$. One may also express $\Delta\Delta G$ in terms of the differential binding of Cl^- and Br^- to each intermediate as

$$\begin{aligned}\Delta\Delta G &= \Delta G(hL, Br^- \rightarrow Cl^-) - \Delta G(hK_L, Br^- \rightarrow Cl^-)\\ &= \Delta\Delta G(hL) - \Delta\Delta G(hK_L),\end{aligned}$$

where $\Delta\Delta G(hK_L)$ and $\Delta\Delta G$(hL) represent the specificity of anion binding in these two photocycle intermediates. These definitions are displayed graphically in Fig. 6.

The implications of $\Delta\Delta G$ can now be understood as a requirement that the binding sites in hK_L and hL are differentially capable of solvating the anion. The present observation, that $\Delta\Delta G > 0$, may be interpreted as either stronger binding of Br^- to hL ($\Delta\Delta G(hL) > 0$, Fig. 6 *A*) or stronger binding of Cl^- to hK_L ($\Delta\Delta G(hK_L) < 0$, Fig. 6 *B*). Because the physiological role of hR is the light-driven transport of Cl^- ions, it at first seems reasonable to interpret $\Delta\Delta G$ in terms of the latter explanation. However, previous results

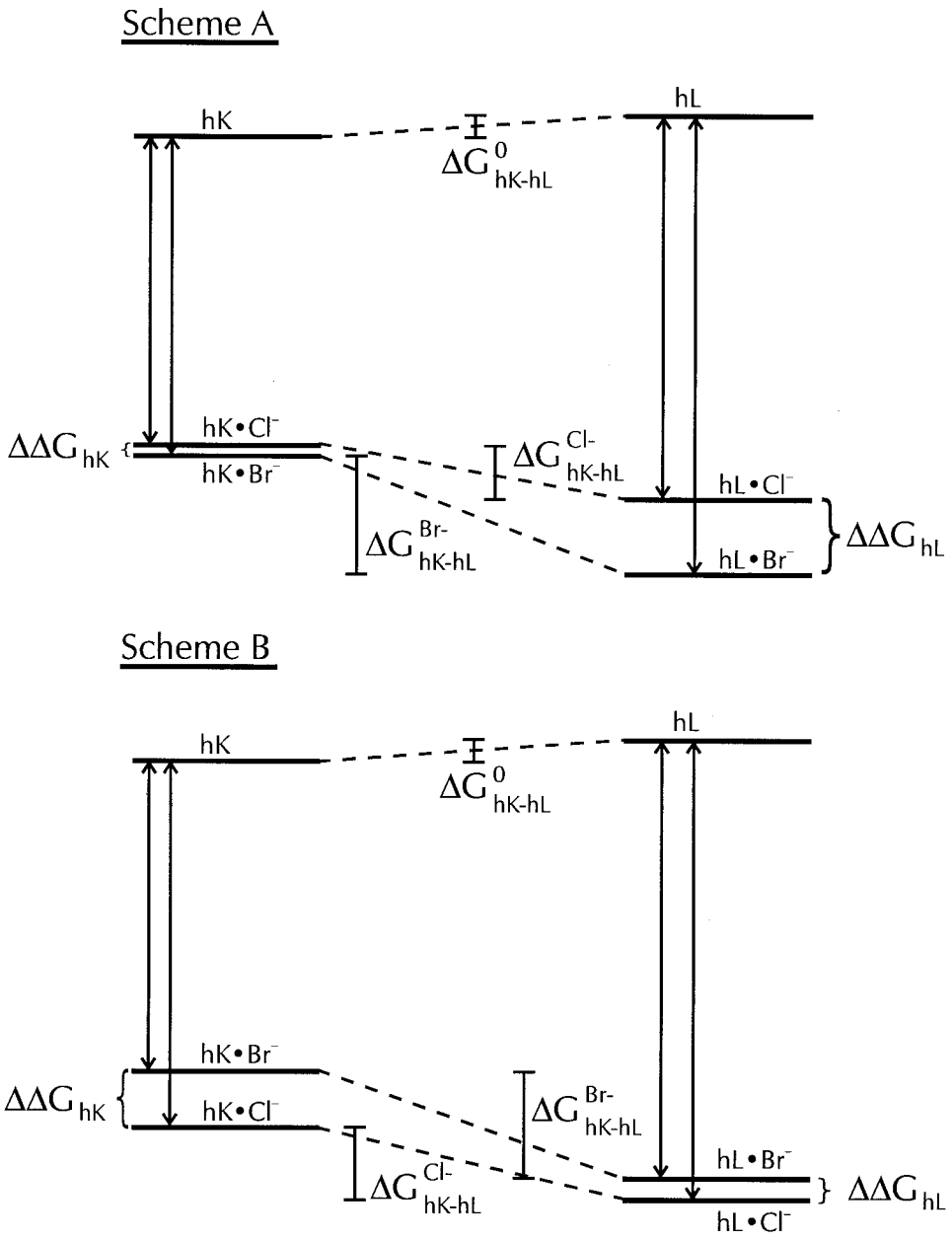

FIGURE 6 Schematic free energy diagrams for the $hK_L \rightleftharpoons hL$ equilibrium and its halide dependence observed in the hR photocycle before the 150-μs decay, with the specificity residing in either (*A*) hL or (*B*) hK_L.

from transport and photocycle assays indicate that the K_d for unphotolyzed hR itself is lower for Br^- than Cl^-, i.e., Br^- binds more tightly than Cl^- to hR, although at most by a factor of 2 (Steiner et al., 1984; Schobert et al., 1983; Rüdiger et al., 1995; Schobert and Lanyi, 1986). This implies that, as defined above, $\Delta\Delta G(hR) > 0$. Unless halide binding to hK_L displays the opposite preference from binding to hR, these earlier results suggest that the main component of $\Delta\Delta G$ responsible for the halide dependence of the hK_L/hL equilibrium comes from the specificity of the hL state.

One study found that the magnitude of the binding free energy for anions (with unphotolyzed hR) is inversely related to the Stokes, or hydrodynamic, radius of the anion (Schobert and Lanyi, 1986). Thus Cl^-, with a larger Stokes radius than Br^- (Nightingale, 1959), binds slightly more weakly to hR. The weakened binding of larger anions was much more pronounced for polyatomic anions, which have much larger Stokes radii (Schobert and Lanyi, 1986).

Although unphotolyzed hR can bind a variety of polyatomic anions, albeit more weakly than halides (Schobert and Lanyi, 1986; Schobert et al., 1983; Steiner et al., 1984), the light-induced generation of the hL state and anion transport by hR are limited almost exclusively to halides and the small anion nitrate (Steiner et al., 1984; Schobert et al., 1983), the latter to an extent that depends greatly on the

species source of the hR (Duschl et al., 1990). The substantial shifts that we observe in the $hK_L \rightleftharpoons hL$ equilibrium depending on the presence of Cl^- or Br^- suggest that this step in the photocycle harbors a specificity for halides. Thus, although a variety of anions may bind to hR and elicit a red-shifted hK state upon photoexcitation (Váró et al., 1995b; Schobert et al., 1983; Steiner et al., 1984), the present results suggest that perhaps only small anions, specifically halides and (to a lesser extent) nitrate, bind strongly enough to hL for this state to be formed during the photocycle. In this scenario, the specificity of transport is not achieved through separate, specific halide binding sites in unphotolyzed hR, as suggested in the two-site model for anion binding to hR (Lanyi et al., 1990). Instead, the anion specificity of the photocycle arises largely from the interactions between the anion and its binding site in the hL state.

Model for halide binding sites in hR and its photoproducts

In consideration of the observed halide dependence in the time-resolved FTIR spectra, as well as a variety of other previous observations, the following model for halide interactions in the hR photocycle up to the hL state can be drawn, as shown in Fig. 7. In the unphotolyzed state the anion is located between, and stabilized by, the positive charges of both the protonated Schiff base and the Arg-108 guanidino group. The anion is closer to the chromophore, affecting the C═C vibrational frequencies and λ_{max} of the chromoprotein, but the anion does not hydrogen-bond directly to the protonated Schiff base, nor to Arg-108. This is consistent with conclusions drawn from the recent atomic-resolution structure of hR (Kolbe et al., 2000). At this point, the anion binding site interactions are not very specific for halides.

Upon photoexcitation, the Schiff base moves to a new location in the hK_L state, disrupting its interaction with the anion and leaving the latter in a position to bind, still with low specificity, at a site whose most important stabilizing Coulombic interaction is now with Arg-108. The anion moves away from Arg-108 to a second site only upon formation of hL, establishing a direct hydrogen bond to the protonated Schiff base (Ames et al., 1992). The key mechanistic conclusions from the present work are that the anion binding site in the hL state is the one with high specificity for halides, and that even halide binding to this side is reversible, permitting re-formation of the hK_L state. Larger anions cannot bind strongly to the hL anion binding site, presumably due to steric constraints, and thus do not complete the normal halide-transporting photocycle. A significant conformational change of the protein backbone is presumably required for the $hK_L \rightarrow hL$ step, but its precise relationship to the vectoriality of transport is unknown.

Our model for halide movement in the hR photocycle (Fig. 7) conflicts somewhat with one previously suggested from the Cl^- concentration dependence of hR photocurrents (Okuno et al., 1999). The previous model featured three halide binding sites: a group of unknown residues near the extracellular surface (site A), Arg-108/Thr-111 (site B), and Thr-203/Arg-200 (site C). In unphotolyzed hR, both sites A and B are occupied with K_d of 60 and 20 mM, respectively, while site C is empty (K_d as high as 7 M). Absorption of a photon leads to a drastic decrease in the halide affinity of site B. Because site A is occupied, the halide moves from site B to site C, from whence it is then released to the cytoplasm. Site B is then re-filled with the halide bound at site A. The cycle is completed by halide uptake from the extracellular medium to site A. The $hK_L \rightarrow hL$ halide movement suggested by the present results and shown in Fig. 7 does not correspond to the movement between any two of these sites. At the very least, the movement of the

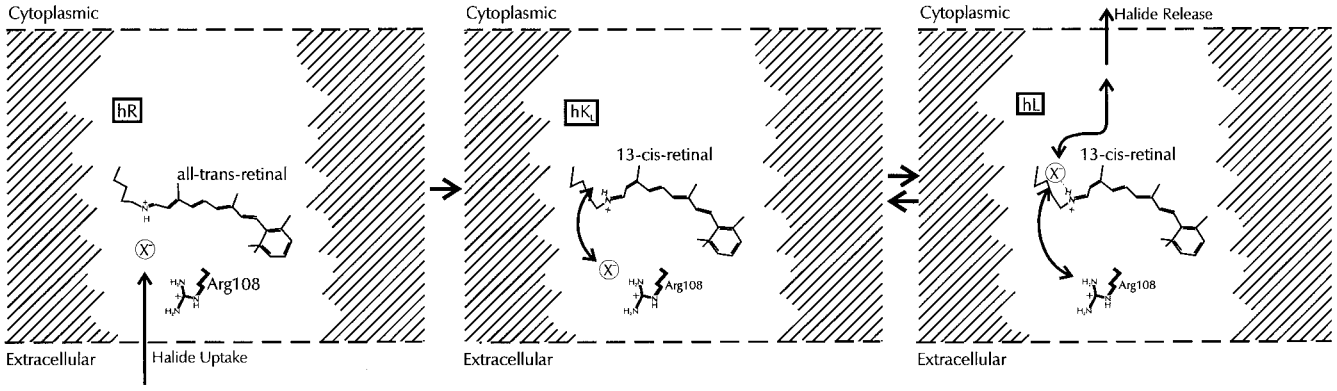

FIGURE 7 Model for halide movements before 1 ms in the hR photocycle based on time-resolved FTIR spectra. The halide, situated in a nonspecific anion binding site in the hR state (*left*), interacts weakly with the Schiff base and with Arg-108. In hK_L, the halide remains behind after the chromophore-protonated Schiff base is repositioned by photoisomerization (*center*), leaving the anion to interact only with Arg-108. These weaker interactions are replaced with a hydrogen-bonded salt bridge to the repositioned protonated Schiff's base in hL (*right*). This contributes to a binding pocket that confers overall specificity for small halides.

bound halide from Arg-108 to the protonated Schiff's base in the $hK_L \rightarrow hL$ transition represents an addition to the previous model (Okuno et al., 1999). In any case, the previously proposed occupation of both sites A and B in the unphotolyzed (hR) state conflicts with the atomic-resolution structure of this state (Kolbe et al., 2000), in which only one Cl^- binding site is observed.

The model in Fig. 7 goes only as far as the hL intermediate. Further movements of the halide in the hN or hO intermediates have been suggested (Rüdiger and Oesterhelt, 1997), but the present data are unable to address these questions due to the unobservability of additional spectral transitions that would allow the FTIR difference spectra of these intermediates to be determined. Analysis of transient visible spectra from *N. pharaonis* hR revealed a 10-times slower, isolated transition between hL and hN in 2 M NaCl (Váró et al., 1995a). At lower Cl^- concentrations, hO accumulates during the same transition (Váró et al., 1995a). Perhaps time-resolved FTIR spectra of this system will be able to determine the difference spectra of hN and hO.

We are grateful to Nicolet Instruments and Bruker Instruments for technical assistance.

This work was supported by grants from the National Institutes of Health (GM-46854) and from Syracuse University. M.S.H. was supported by National Institutes of Health Predoctoral Training Grant GM-08323. Support for specialized instrumentation came from the W. M. Keck Foundation.

REFERENCES

Ames, J. B., J. Raap, J. Lugtenburg, and R. A. Mathies. 1992. Resonance Raman study of halorhodopsin photocycle kinetics, chromophore structure, and chloride-pumping mechanism. *Biochemistry.* 31:12546–12554.

Bivin, D., and W. Stoeckenius. 1986. Photoactive retinal pigments in haloalkaliphilic bacteria. *J. Gen. Microbiol.* 132:2167–2177.

Braiman, M. S., P. L. Ahl, and K. J. Rothschild. 1987. Millisecond Fourier-transform infrared difference spectra of bacteriorhodopsin's M412 photoproduct. *Proc. Natl. Acad. Sci. USA.* 84:5221–5225.

Braiman, M. S., T. J. Walter, and D. M. Briercheck. 1994. Infrared spectroscopic detection of light-induced change in chloride-arginine interaction in halorhodopsin. *Biochemistry.* 33:1629–1635.

Chen, W.-G., and M. S. Braiman. 1991. Kinetic analysis of time-resolved infrared difference spectra of the L and M intermediates of bacteriorhodopsin. *Photochem. Photobiol.* 53:905–910.

Chizhov, I. V., D. S. Chernavskii, M. Engelhard, K.-H. Müller, B. V. Zubov, and B. Hess. 1996. Spectrally silent transitions in the bacteriorhodopsin photocycle. *Biophys. J.* 71:2329–2345.

Chon, Y. S., H. Kandori, J. Sasaki, J. K. Lanyi, R. Needleman, and A. Maeda. 1999. Existence of two L photointermediates of halorhodopsin from *Halobacterium salinarium*, differing in their protein and water FTIR bands. *Biochemistry.* 38:9449–9455.

Dioumaev, A. K. 1997. Evaluation of intrinsic chemical kinetics and transient photoproduct spectra from time-resolved spectroscopic data. *Biophys. Chem.* 67:1–26.

Dioumaev, A. K., and M. S. Braiman. 1997a. Nano- and microsecond time-resolved FTIR spectroscopy of the halorhodopsin photocycle. *Photochem. Photobiol.* 66:755–763.

Dioumaev, A. K., and M. S. Braiman. 1997b. Two bathointermediates of the bacteriorhodopsin photocycle, distinguished by nanosecond time-resolved FTIR spectroscopy at room temperature. *J. Phys. Chem. B.* 101:1655–1662.

Duschl, A., J. K. Lanyi, and L. Zimányi. 1990. Properties and photochemistry of a halorhodopsin from the haloalkalophile, *Natronobacterium pharaonis. J. Biol. Chem.* 265:1261–1267.

Duschl, A., M. A. McCloskey, and J. K. Lanyi. 1988. Functional reconstitution of halorhodopsin, properties of halorhodopsin-containing proteoliposomes. *J. Biol. Chem.* 263:17016–17022.

Fodor, S. P., R. A. Bogomolni, and R. A. Mathies. 1987. Structure of the retinal chromophore in the hRL intermediate of halorhodopsin from resonance Raman spectroscopy. *Biochemistry.* 26:6775–6778.

Gerscher, S., M. Mylrajan, P. Hildebrandt, M. H. Baron, R. Müller, and M. Engelhard. 1997. Chromophore-anion interactions in halorhodopsin from *Natronobacterium pharaonis* probed by time-resolved resonance Raman spectroscopy. *Biochemistry.* 36:11012–11020.

Hazemoto, N., N. Kamo, Y. Kobatake, M. Tsuda, and Y. Terayama. 1984. Effect of salt on photocycle and ion-pumping of halorhodopsin and third rhodopsinlike pigment of *Halobacterium halobium. Biophys. J.* 45: 1073–1077.

Hessling, B., G. Souvignier, and K. Gerwert. 1993. A model-independent approach to assigning bacteriorhodopsin's intramolecular reactions to photocycle intermediates. *Biophys. J.* 65:1929–1941.

Heymann, J. A., W. A. Havelka, and D. Oesterhelt. 1993. Homologous overexpression of a light-driven anion pump in an archaebacterium. *Mol. Microbiol.* 7:623–630.

Kolbe, M., H. Besir, L.-O. Essen, and D. Oesterhelt. 2000. Structure of the light-driven chloride pump halorhodopsin at 1.8 Å resolution. *Science.* 288:1390–1396.

Lanyi, J. K. 1984. Light-dependent *trans* to *cis* isomerization of the retinal in halorhodopsin. *FEBS Lett.* 175:337–342.

Lanyi, J. K., A. Duschl, G. Váró, and L. Zimányi. 1990. Anion binding to the chloride pump, halorhodopsin, and its implications for the transport mechanism. *FEBS Lett.* 265:1–6.

Lozier, R. H., R. A. Bogomolni, and W. Stoeckenius. 1975. Bacteriorhodopsin: a light-driven proton pump in *Halobacterium halobium. Biophys. J.* 15:955–962.

Malinowski, E. H., and D. G. Howery. 1980. Factor Analysis in Chemistry. John Wiley and Sons, New York.

Nightingale, E. R., Jr. 1959. Phenomenological theory of ion solvation. Effective radii of hydrated ions. *J. Phys. Chem.* 63:1381–1387.

Okuno, D., M. Asaumi, and E. Muneyuki. 1999. Chloride concentration dependency of the electrogenic activity of halorhodopsin. *Biochemistry.* 38:5422–5429.

Pande, C., J. K. Lanyi, and R. H. Callender. 1989. Effects of various anions on the Raman spectrum of halorhodopsin. *Biophys. J.* 55:425–431.

Polland, H. J., M. A. Franz, W. Zinth, W. Kaiser, P. Hegemann, and D. Oesterhelt. 1985. Picosecond events in the photochemical cycle of the light-driven chloride-pump halorhodopsin. *Biophys. J.* 47:55–59.

Rödig, C., and F. Siebert. 1999. Errors and artifacts in time-resolved step-scan FT-IR spectroscopy. *Appl. Spectrosc.* 53:893–901.

Rothschild, K. J., O. Bousché, M. S. Braiman, C. A. Hasselbacher, and J. L. Spudich. 1988. Fourier transform infrared study of the halorhodopsin chloride pump. *Biochemistry.* 27:2420–2424.

Rüdiger, M., U. Haupts, K. Gerwert, and D. Oesterhelt. 1995. Chemical reconstitution of a chloride pump inactivated by a single point mutation. *EMBO J.* 14:1599–1606.

Rüdiger, M., and D. Oesterhelt. 1997. Specific arginine and threonine residues control anion binding and transport in the light-driven chloride pump halorhodopsin. *EMBO J.* 16:3813–3821.

Schobert, B., and J. K. Lanyi. 1982. Halorhodopsin is a light-driven chloride pump. *J. Biol. Chem.* 257:10306–10313.

Schobert, B., and J. K. Lanyi. 1986. Electrostatic interaction between anions bound to site I and the retinal Schiff base of halorhodopsin. *Biochemistry.* 25:4163–4167.

Schobert, B., J. K. Lanyi, and E. J. Cragoe, Jr. 1983. Evidence for a halide-binding site in halorhodopsin. *J. Biol. Chem.* 258:15158–15164.

Sharonov, A. Y., N. V. Tkachenko, V. V. Savransky, and A. K. Dioumaev. 1991. Time-resolved ultraviolet absorption changes in the photocycle of bacteriorhodopsin. *Photochem. Photobiol.* 54:889–895.

Spencer, D. B., and T. G. Dewey. 1990. Activation parameters for the halorhodopsin photocycle: a phase lifetime spectroscopic study of the 520- and 640-nanometer intermediates. *Biochemistry.* 29:3140–3145.

Steiner, M., D. Oesterhelt, M. Ariki, and J. K. Lanyi. 1984. Halide binding by the purified halorhodopsin chromoprotein. I. Effects on the chromophore. *J. Biol. Chem.* 259:2179–2184.

Váró, G., L. S. Brown, J. Sasaki, H. Kandori, A. Maeda, R. Needleman, and J. K. Lanyi. 1995a. Light-driven chloride ion transport by halorhodopsin from *Natronobacterium pharaonis.* 1. The photochemical cycle. *Biochemistry.* 34:14490–14499.

Váró, G., L. Zimányi, X. Fan, L. Sun, R. Needleman, and J. K. Lanyi. 1995b. Photocycle of halorhodopsin from *Halobacterium salinarium. Biophys. J.* 68:2062–2072.

Walter, T. J., and M. S. Braiman. 1994. Anion-protein interactions during halorhodopsin pumping: halide binding at the protonated Schiff base. *Biochemistry.* 33:1724–1733.

Zimányi, L., L. Keszthelyi, and J. K. Lanyi. 1989. Transient spectroscopy of bacterial rhodopsins with an optical multichannel analyzer. 1. Comparison of the photocycles of bacteriorhodopsin and halorhodopsin. *Biochemistry.* 28:5165–5172.

Zimányi, L., and J. K. Lanyi. 1989a. Low-temperature photoreactions of halorhodopsin. 2. Description of the photocycle and its intermediates. *Biochemistry.* 28:1662–1666.

Zimányi, L., and J. K. Lanyi. 1989b. Transient spectroscopy of bacterial rhodopsins with an optical multichannel analyzer. 2. Effects of anions on the halorhodopsin photocycle. *Biochemistry.* 28:5172–5178.